Journal of the Indian Society of Remote Sensing (February 2020) 48(2):249–262
https://doi.org/10.1007/s12524-019-01042-1

RESEARCH ARTICLE

Identification of Sugarcane with NDVI Time Series Based on HJ-1 CCD and MODIS Fusion

Yanli Chen[1,2] · Liping Feng[1] · Jianfei Mo[2] · Weihua Mo[2] · Meihua Ding[2] · Zhiping Liu[2]

Received: 28 November 2018 / Accepted: 3 September 2019 / Published online: 25 November 2019

Abstract

It is currently difficult to acquire the clear-sky data with high spatial resolutions in spring and summer in the southern region of China, making it impossible to carry out timely and fine monitoring of sugarcane planting information. Thus, Fusui, a sugarcane producing county in Guangxi, was selected in this paper to analyze the NDVI characteristics and change rules during the whole growth period of sugarcane based on MODIS and HJ-1 CCD remote sensing data, which were fused into 30 m resolution NDVI time series data with high accuracy by using the spatial and temporal fusion model of multi-source remote sensing data ESTRAFM. In addition, the NDVI change rate and sample automatic training threshold were used to construct the sugarcane planting information identification model. The results showed that the fused images showed a high similarity with the observed images, indicating good fusion quality. Moreover, the correlation coefficients in the sugarcane planting area reached 0.953, and AD, AAD and SD were 0.033, 0.019 and 0.007, respectively. The NDVI change rate model was used to identify the sugarcane planting information in different time phases of 113 d, 129 d, 145 d, 193 d and 209 d in spring and summer, and the overall accuracy was 92.17%, 92.58%, 91.78%, 90.52% and 91.17%, respectively. The established model also achieved good results in 2017 with the overall accuracies are 88.44%, 87.79%, 89.79%, 88.34% for 113 d, 145 d, 193 d and 209 d.

Keywords Sugarcane identification · Space–time fusion · NDVI time series · HJ-CCD · MODIS

Introduction

The identification of crop planting information is of great significance to agricultural production management, sustainable agricultural development and national food security, and remote sensing technology has become an important means to quickly acquire information on the temporal and spatial distribution of crops. At present, optical remote sensing data is the main data source for crop information extraction. The identification methods mainly include computer supervised classification, multi-temporal analysis and object-oriented classification. Although microwave remote sensing data can overcome the effects of cloudy and rainy weather, it is difficult to promote and apply due to technical and cost restrictions. Sugarcane is an important raw material for sugar production. More than 50% of the world's sugar comes from sugarcane. China is the third largest sugarcane producer in the world after Brazil and India. For China, more than 80% sugar comes from sugarcane from 2003, which is far higher than the world average level of 50%. Grasping sugarcane planting area in time is of important significance for the stability of sugar market, agricultural production and regional economic development (Tan et al. 2007). There are quite a lot reports on the current mainstream crop information identification methods which can identify sugarcane and the area estimation accuracy can reach up to 90%. In these reports, data sources selected include MODIS (Tan et al. 2007; Alexandre et al. 2006), HJ-1 (Ma et al. 2011; Ding et al. 2012; Wang et al. 2014; Zhou et al. 2016), GF-1 (Liu et al. 2014), Landsat-8 OLI (Chen et al. 2015), Landsat-7 ETM+ (Fortes and Demattê 2006; Vieira et al. 2012), SAR

✉ Yanli Chen
cyl0505@sina.com

[1] College of Resources and Environmental Sciences, China Agricultural University, Beijing 100193, China

[2] Guangxi Institute of Meteorological Sciences, Remote Sensing Application Test Base of the National Satellite Meteorological Center of China, Nanning 530022, China

(Lin et al. 2009), and classification methods adopted include supervised classification (Tan et al. 2007), unsupervised classification (Alexandre et al. 2006), decision tree (Liu et al. 2014), object-oriented classification (Wang et al. 2014; Zhou et al. 2016; Vieira et al. 2012) or combination of multiple methods (Ma et al. 2011; Ding et al. 2012; Chen et al. 2015). The sugarcane planting areas in China are mainly distributed in Guangxi, Yunnan, Hainan and Guangzhou. Affected by cloudy and rainy weather and satellite revisiting cycles, it is difficult to obtain large-scale clear-sky images with high spatial resolution in spring and summer (here use Chinese lunar calendar division method, spring is from march to may and summer is from June to August) in these areas, so the existing research on optical remote sensing-based sugarcane classification mainly relies on clear-sky remote sensing images in October and November. Therefore, reconstructing the high spatial resolution data series of sugarcane planting area and constructing a sugarcane identification model based on new series can provide an effective way for timely and refined monitoring of sugarcane planting information in spring and summer.

As a matter of fact, time series data has become a hot topic in crop classification research. Jakubauskas et al. (2002) used the AVHRR NDVI time series data to classify corn, soybean and alfalfa crops by harmonic algorithm. Zhang et al. (2008) achieved the land cover classification in North China by using the decision tree algorithm based on MODIS EVI time series data. Miao et al. (2011) reconstructed the MODIS NDVI time series data by S-G filtering algorithm and completed the extraction of regional rice planting area information. Yang et al. (2015) remodeled the GF-1 NDVI time series data by using harmonic algorithm to study the effectiveness of various classification methods for winter wheat–summer corn, corn and rice. Li et al. (2013) rebuilded HJ-1 time series data by using the spline algorithm and carried out the classification and identification of soybean, corn, rice and cushaw. The spatial resolution of existing time-sensitive remote sensing data is generally low, and the acquisition period of high spatial resolution remote sensing data is long. Affected by topography and landform, there are few large-scale areas in the main sugarcane producing areas in southern China. Thus, the various factors lead to the fact that the single source of data is difficult to meet the demand for high-temporal resolution remote sensing data to obtain the sugarcane planting information under complex weather and terrain conditions in southern China. Therefore, there are few reports on sugarcane classification using NDVI time series data. In order to solve the problem of insufficient satellite remote sensing data acquisition ability, scholars have proposed a technology that can combine high-temporal resolution features of low spatial resolution remote sensing data with high spatial resolution features of medium and high spatial resolution remote sensing data, namely, the multi-source remote sensing data spatiotemporal fusion technology. Gao et al. (2006) proposed the spatial and temporal adaptive reflectance fusion model STARFM in 2006, and Zhu et al. (2010) proposed the enhanced spatial and temporal adaptive reflectance fusion model ESTARFM in 2010. Both models have been widely applied, and the application of the 2 spatiotemporal fusion models is focused on MODIS-Landsat remote sensing data (Gao et al. 2006; Zhu et al. 2010). So far, only Sun et al. (2016) have reestablished the NDVI series with STRAFM based on HJ-1 CCD and MODIS data and verified the effectiveness of STRAFM on HJ-1 CCD and MODIS data fusion. However, there is still no report on the application of the ESTRAFM model in HJ-1 CCD data. The fused NDVI series has made some progress in crop monitoring. Cai et al. (2012) studied the adaptability of MODIS and Landsat data fusion in crop monitoring, finding that the reflectance of fusion image of corn and cotton was similar to that of the observed image. In addition, the time series images based on MODIS-Landsat fusion have been successfully applied to the extraction of rice planting area (Zhang and Zeng 2015; Wu et al. 2010). However, there is no report on the application of this technology in sugarcane.

Through the review of the existing research, we know that in order to monitor the spring and summer sugarcane planting information in south China, it is necessary to generate a high-resolution NDVI time series. Therefore, in this study, the MODIS and HJ-1 CCD remote sensing data and fusion model ESTRAFM are used to obtain 30 m resolution NDVI time series. On the basis of this, the spectral characteristics and change rules of sugarcane in the whole growth period were analyzed, and the sugarcane identification model based on NDVI time series data was constructed, with the aim to provide scientific references for the refined monitoring of sugarcane by improving and enhancing the use of remote sensing technology.

Test Area

The test area was in Fusui County, southwest of Guangxi Province. It is a famous sugarcane producing base in Guangxi. Located at the center coordinates of 107°6′0.38″ E, 25°1′8.69″ N with area about 160 km^2, it is a subtropical humid monsoon region with an average annual temperature of 21.7 °C, annual average rainfall of about 1 300 mm, flat elevation of less than 200 m and annual frost-free period of more than 342 d. Sugarcane has a long growth period span, usually planted in mid-March, emerged in late March, entering the tillering stage in mid-May and stem elongation

period in late June, and mid-November is the technical maturing stage. The main crops in the corresponding period are early rice, late rice, spring corn and autumn corn. Early rice is planted in mid-March and matures in early July; late rice is planted in mid-July and matures in early November; spring corn is planted in mid-February, matures in late June; autumn corn is planted in late July and matures in early December (Table 1, Fig. 1).

Data and Methods

Data Sources and Pre-processing

HJ-1 CCD data: the systematically geometric corrected level-2 product data downloaded from China Center for Resources Satellite Data and Application. There were a total of 4 bands (spectrum range of 0.43–0.52 μm, 0.52–0.60 μm, 0.63–0.69 μm, 0.76–0.90 μm) with the spatial resolution of 30 m. The product data was sequentially subjected to radiometric calibration, atmospheric

Table 1 Phenological calendar of main crops in Fusui County

	Early rice	Late rice	Sugarcane	Spring corn	Autumn corn
February					
Middle				Sowing	
Late				Emergence	
March					
Early				Three-leaf stage	
Middle	Sowing–seeding		Sowing		
Late	Three-leaf stage		Emergence	Seven-leaf stage	
April					
Early	Transplanting-greening back				
Middle	Tillering			Jointing stage	
Late					
May					
Early	Jointing stage				
Middle			Tillering	Silking stage	
Late	Booting stage			Milk-ripe stage	
June					
Early	Heading stage				
Middle	Milk-ripe stage				
Late			Stem elongation	Mature stage	
July					
Early	Mature stage				
Middle		Sowing–seeding			
Late		Three-leaf stage			Sowing
August					
Early		Transplanting-greening back			Emergence
Middle		Tillering			
September					
Early		Jointing stage			
Late		Booting stage			Tasseling stage
October					
Early		Heading stage			Silking stage
Middle		Milk-ripe stage			
November					
Early		Mature stage			
Middle			Technical maturity		
December					
Early					Mature stage

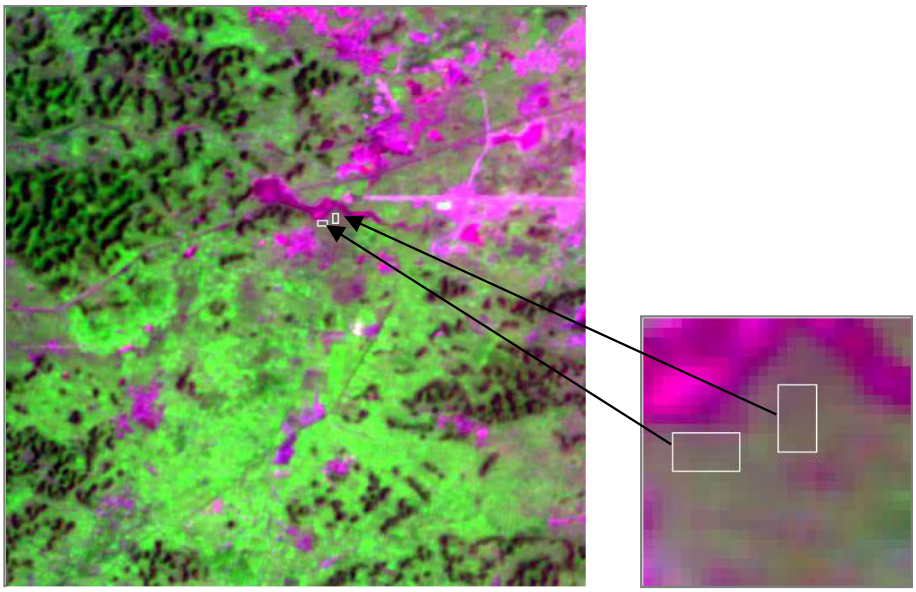

Fig. 1 Schematic diagram of test area and sugarcane samples (inside the white border, magnify 7 times)

correction, geometric correction to obtain reflectance data, and NDVI corresponding to the date was calculated. Radiation calibration was performed using the 2011 HJ-1 A/B star absolute radiometric calibration coefficient provided by the China Center for Resources Satellite Data and Application; the geometric correction reference image was Landsat TM in 2008, and the rectification error was less than 0.5 pixels by using cubic convolution algorithm through selecting the ground control point GCP. The atmospheric correction adopted the FLAASH module. ENVI 5.0 was selected to perform the above processing, and the image coordinate system was UTM-WGS84.

MODIS data: the global vegetation index product MOD13Q1 was downloaded from NASA's official website, with 250 m resolution and 16 d synthesis cycle, a total of 23 scenes of a year. The MRT (MODIS Reprojection Tool) software provided by USGS was used to perform projection conversion and resampling processing on the product data to ensure that it had the same coordinate system and spatial resolution as the HJ-1 CCD data.

As the preliminary processing was carried out for the data of the whole swath, in order to make the data entering the ESTRAFM model contained only the test area, finally, the HJ-1 CCD and MOD13Q1 data were cropped to obtain the red band, near-infrared band and NDVI images of the test area. Details of MODIS and HJ-1 CCD were given in Table 2.

Field sampling data: combined with the digital elevation model DEM in the test area, field sampling of sugarcane, rice, corn, forest, towns, water bodies and other ground objects was carried out on September 5, October 23, 2011, May 14, 2017. In order to improve the reliability of the verification data, the sugarcane planting plot with an area larger than 60 m × 60 m was selected as the sample area, and a hand-held GPS (GPSMap 629sc) was used to record the position and measure the area of the sample area. A total of 55 representative sugarcane sample areas were selected.

Table 2 Properties of HJ-1 CCD and MODIS

	HJ-1 CCD	MODIS
Orbital altitude	649 km	705 km
Resolution	30 m	250 m
Swath	8/90	H27v06
	7/90	
Revisit date	4–8 d	1 d
Passing territory time	11:30	11:00
Visible spectrum	0.43–0.52 μm	0.62–0.67 μm (250 m)
	0.52–0.60 μm	0.84–0.88 μm (250 m)
	0.63–0.69 μm	
	0.76–0.90 μm	

Methods

ESTRAFM Spatial and Temporal Fusion Model

The ESTARFM (Enhanced Spatial and Temporal Adaptive Reflectance Fusion Model) is proposed by Zhu et al. (2010). The algorithm assumes that the reflectance $F(x_i, y_i, t_k)$ of a pixel in the high-resolution image had the following relationship with the reflectance $C(x_i, y_i, t_k)$ in the low-resolution image at the same moment t_k:

$$F(x_i, y_i, t_k) = a \times C(x_i, y_i, t_k) + b \quad (1)$$

where a and b are linear fit coefficients. The values of a and b could be solved through 2 sets of high–low resolution

images of the same periods, and then the high-resolution image of any period could be predicted by the data of one of the period:

$$F(x_i, y_i, t_P) = F(x_i, y_i, t_0) + \upsilon(x_i, y_i) \times (C(x_i, y_i, t_P) - C(x, y, t_0)) \quad (2)$$

where t_P and t_0 are the acquisition time of the images of the 2 periods; $\upsilon(x_i, y_i)$ is a conversion coefficient equivalent to a at the point (x_i, y_i). In a given moving window, the reflectance value of the center pixel of the predicted image could be calculated by neighboring spectra similar pixels:

$$F\left(x_{\omega/2}, y_{\omega/2}, t_P, B\right) = F\left(x_{\omega/2}, y_{\omega/2}, t_0, B\right) + \sum_{i=1}^{N} W_i \times V_i \times (C(x_i, y_i, t_P, B) - C(x_i, y_i, t_0, B)) \quad (3)$$

where ω is the width of the moving window; $\left(x_{\omega/2}, y_{\omega/2}\right)$ is the central pixel coordinate; (x_i, y_i) is the ith spectral similar pixel coordinate; N is the number of similar pixels; V_i is the conversion coefficient of the ith similar pixel; W_i is the weight coefficient of the ith similar pixel to the central pixel, which is calculated from the spectral distance weight, temporal distance weight and spatial distance weight of the similar pixels in the moving window, and the specific calculation method is referred to that of Zhu et al. (2010).

Construction Method of Sugarcane Identification Model

ESTRAFM was used to perform the fusion of HJ-1 CCD and MOD13Q1 data, to obtain the NDVI series of 30 m resolution in the test area of 2011 and 2017. Table 3 lists ESTRAFM's input, output and validation data. The data of 2011 were used to establish sugarcane identification model and indicators, and the data of 2017 were used for verification of the established model. The spectral characteristics and change rules of sugarcane, rice and corn were analyzed according to the ground sampling points in the field. And the NDVI change rate and sample automatic training threshold were used to construct the sugarcane planting information identification model.

Results and Analysis

NDVI fused Image Evaluation

The ESTRAFM spatiotemporal fusion algorithm was used to get the fused images with the corresponding date of MOD13Q1. The input image was the HJ-1CCD, MOD13Q1 data pair and the MOD13Q1 data of the needed fusion date. The fused image obtained by ESTRAFM was visually inspected. The red, near-infrared bands and NDVI images of the observed HJ-1 CCD showed good consistent with the red, near-infrared bands and NDVI images of the ESTRAFM fused images in spatial distribution. ESTRAFM captured the detail spatial distribution characteristics of the observed HJ-1 CCD image. After fusion, the images were clear, and there were clear boundaries between different surface types, which showed very small difference from the observed images (Figs. 2, 3 and 4).

The fusion effect of ESTRAFM on the observed images was quantitatively analyzed by using the evaluation indicators of correlation coefficient R, average absolute difference (AAD), average difference (AD) and standard

Table 3 Input, output and validation data of ESTRAFM

	Input data		Output data (predicted HJ-1 CCD images)	Validation data (real HJ-1 CCD images)
	Real HJ-1CCD images	Real MODIS images		
2011	2011-08-29	2011-08-29	A total of 23 scenes of a year	2011-04-19
	2011-11-24	2011-11-24		2011-05-28
		A total of 23 scenes of a year		2011-09-30
				2011-10-17
				2011-11-12
2017	2017-02-19	2017-02-19	97 d	
	2011-09-16	2011-09-16	113 d	
		97 d	145 d	
		113 d	193 d	
		145 d	209 d	
		193 d		
		209 d		

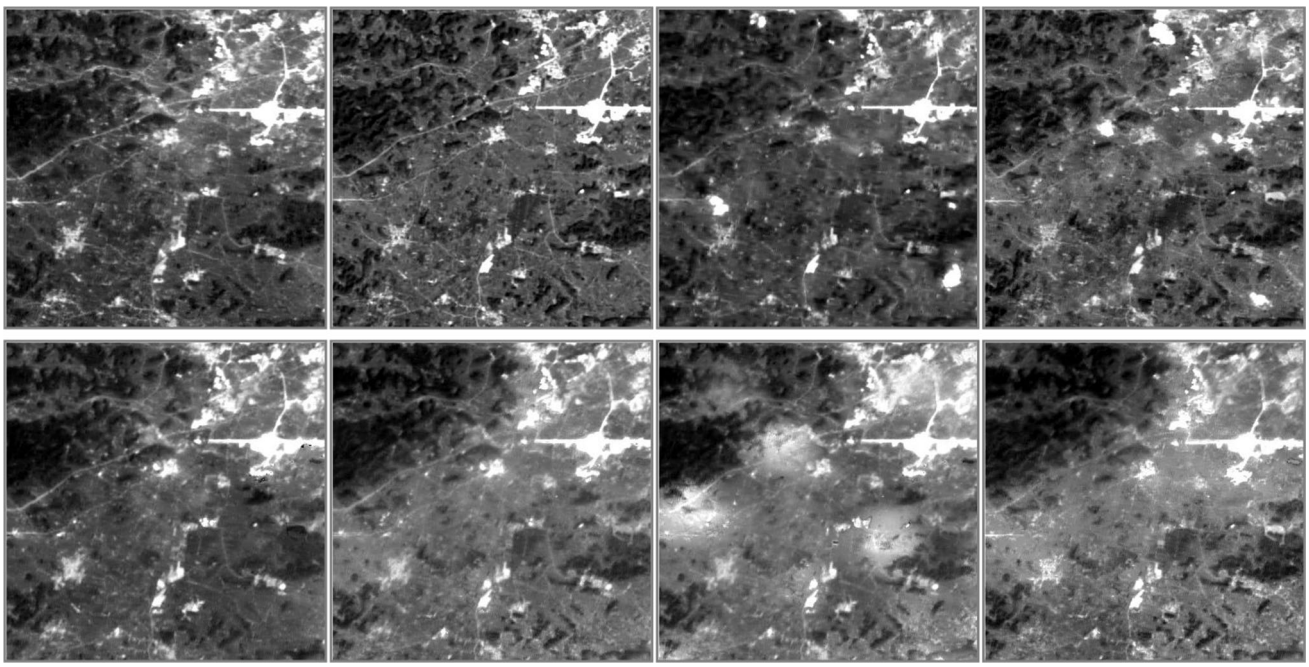

Fig. 2 Comparison of the observed image and the fused image in the near-infrared band (top: observed image, bottom: ESTRAFM predicted image, image date: from the left to right: 2011-04-19, 2011-05-28, 2011-09-30, 2011-10-17)

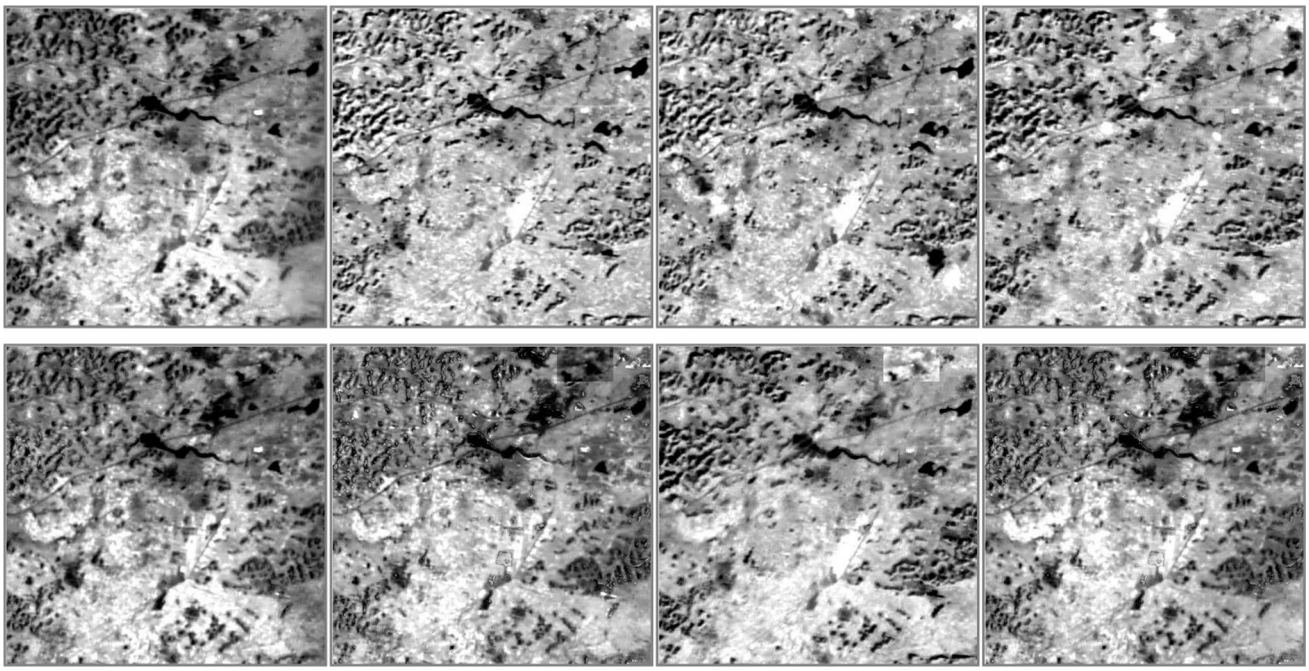

Fig. 3 Comparison of the observed image and the fused image in the red band (top: observed image, bottom: ESTRAFM predicted image, image date: from the left to right: 2011-04-19, 2011-05-28, 2011-09-30, 2011-10-17)

deviation (SD). The ESTRAFM fused images were highly correlated with the observed HJ-1CCD images. The average correlation coefficients of red, near-infrared and NDVI were 0.930, 0.885 and 0.840, respectively. The AD, AAD and SD were small for both the fused and observed images in differencing images. The fused image of sugarcane sample areas had high similarity with the observed image with the correlation coefficient reaching 0.953, and AD, AAD and SD of 0.033, 0.019 and 0.007, respectively (Table 4 and Fig. 5).

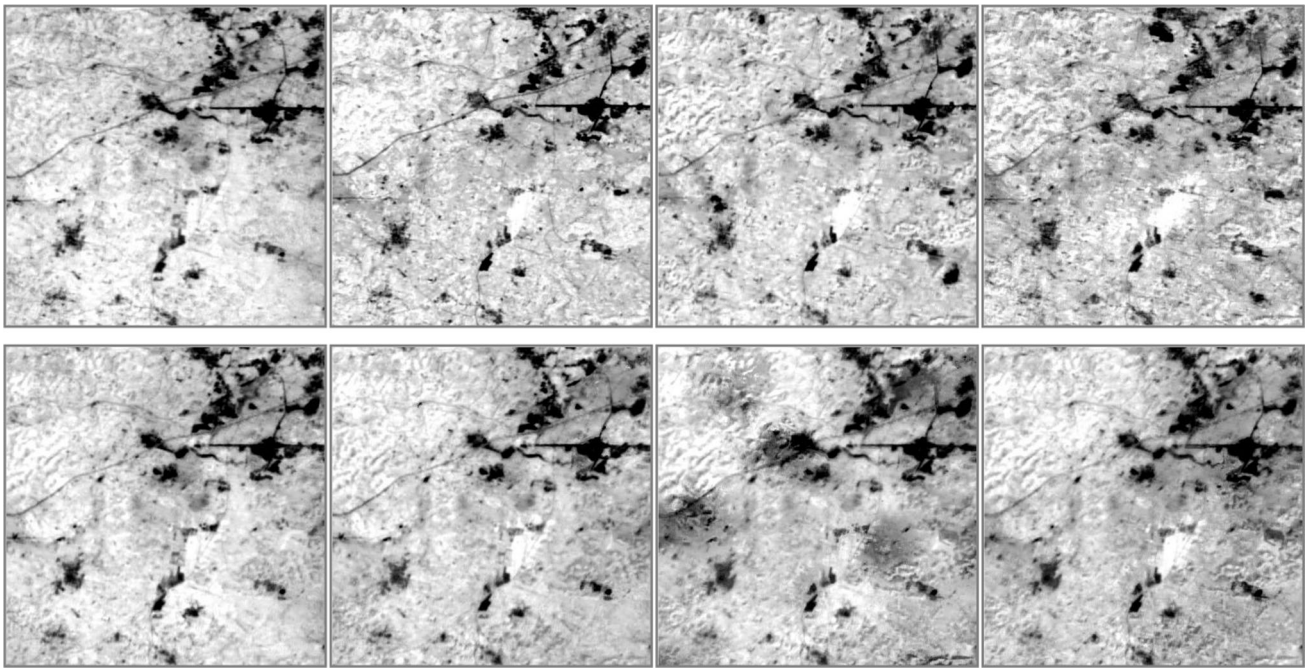

Fig. 4 Comparison of the observed image and NDVI fused image. Top: observed image, bottom: ESTRAFM predicted image, image date: from the left to right: 2011-04-19, 2011-05-28, 2011-09-30, 2011-10-17

Sugarcane Extraction Model

Analysis on Spectral Characteristics of Sugarcane

The curves of NDVI changes of different ground features in the test area could be obtained by using the typical ground features in field sampling and the NDVI series from ESTRAFM fusion (Figs. 6 and 7). During the growth period of plants, NDVI can show regular increases and decreases. Since the main purpose of this study was to realize the identification of sugarcane in spring and summer, only the NDVI change rules of related crops before July were analyzed in detail. For sugarcane, the vegetation coverage was low from January to mid-March (1–113 d), so NDVI series changed little; from mid-March to late June was the initial stage of stem elongation (113–177 d), and NDVI increased rapidly; from late June to early October was the transition from stem elongation to sugar accumulation stage (177–273 d), and NDVI increased slowly; after early October (273 d), sugarcane came to the transition from sugar accumulation to technical maturing stage, and the NDVI began to decline. For early rice, the NDVI increased quickly from early April to early May (97–129 d) and then decreased quickly from early May to late July (129–209 d). For spring corn, NDVI increased rapidly from mid-January to late June (17–177 d) and then decreased from late June to late July (177–209 d). The NDVI value of the forest was high, and the change was not significant during the whole growth period. Through the whole growth period, sugarcane only showed great distinction degree with early rice, spring corn and forest from late April to late May (113–145 d), which was 1 month after emergence and about half a month after tillering. However, this time period was under the effect of weather and data revisiting cycles, making it extremely hard to obtain high spatial resolution clear-sky data. Moreover, it was almost impossible to achieve the accurate identification of sugarcane due to the differences in seeding and growth vigor. In other periods, sugarcane was mingled with rice, corn and forest to different degrees. For example, in late July (209 d), the NDVI of corn and rice had a distinct trough, which was just the harvesting stage of early rice and spring corn. The NDVI of sugarcane had low mingling degree with the NDVI of spring corn but very close to the NDVI of forest.

Construction of Sugarcane Identification Model

According to the NDVI change rules of sugarcane in spring and summer, the sugarcane identification model could be constructed by using the remote sensing data of sugarcane in different time phases through the NDVI change rate:

$$V = \frac{\mathrm{NDVI_t} - \mathrm{NDVI_s}}{D} \tag{4}$$

where $\mathrm{NDVI_t}$ and $\mathrm{NDVI_s}$. are the NDVI of sugarcane at two different time phases; D is the number of days in which the NDVI of the 2 time phases are different. Since

Table 4 Accuracy evaluation of fused images

Wave band	*R*	AD	AAD	SD
Near infrared	0.930	− 0.005	0.013	0.017
Red light	0.885	− 0.020	0.021	0.009
NDVI	0.840	0.048	0.066	0.050
Sugarcane sampling plot	0.953	0.033	0.019	0.007

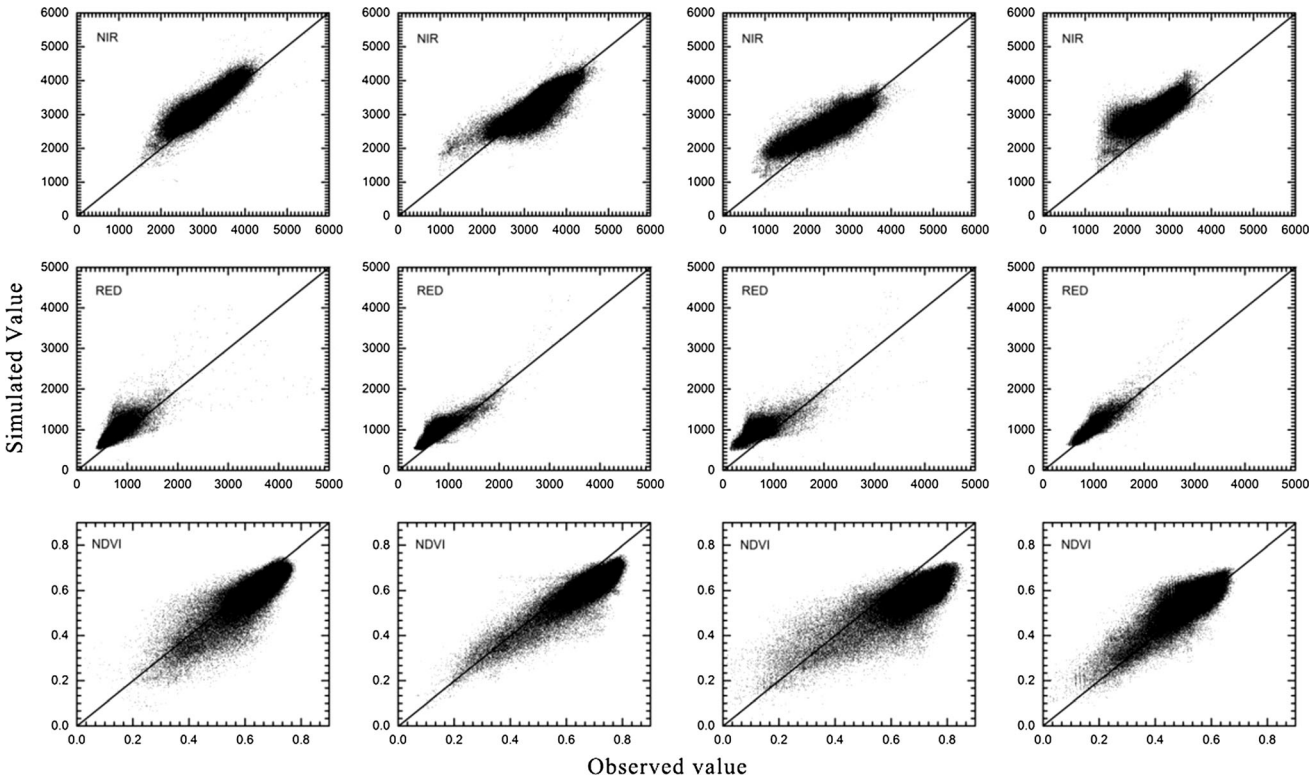

Fig. 5 Scatter plots of observed image and fused (image date: from the left to right: 2011-04-19, 2011-05-28, 2011-09-30, 2011-10-17)

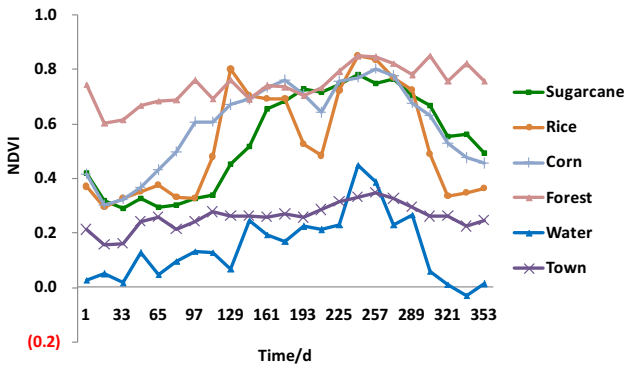

Fig. 6 Curves of NDVI changes for different surface features in the test area

sugarcane in Guangxi is generally emerged in late March, combined with its NDVI change rules, the corresponding period of s in this study is 97 d, and the corresponding phases of t are 113 d, 129 d, 145 d, 161 d, 177 d, 193 d, 209 d, 225 d.

There were a total of 9 periods of NDVI images after ESTRAFM fusion, namely, 113 d, 129 d, 145 d, 161 d, 177 d, 193 d, 209 d and 225 d. The NDVI change rates of vegetation at different time phases were plotted based on the analysis of the maximum (max), minimum (min) and mean values of sugarcane, rice, corn and forest collected from the sampling points in field (Fig. 8). Thus, the changes of NDVI of different vegetation types were studied. In periods 97–161 d, 97–177 d, the NDVI of both sugarcane and early rice were in the period of rapid, and the NDVI change rates of the 2 were very close, making it difficult to distinguish sugarcane. While in other periods, sugarcane could be well identified by the NDVI change rate and sample automatic training threshold (Table 5).

Evaluation of Sugarcane Identification Accuracy

The sugarcane in the test area was identified by using the fused remote sensing images in the 6 periods of 97 d,

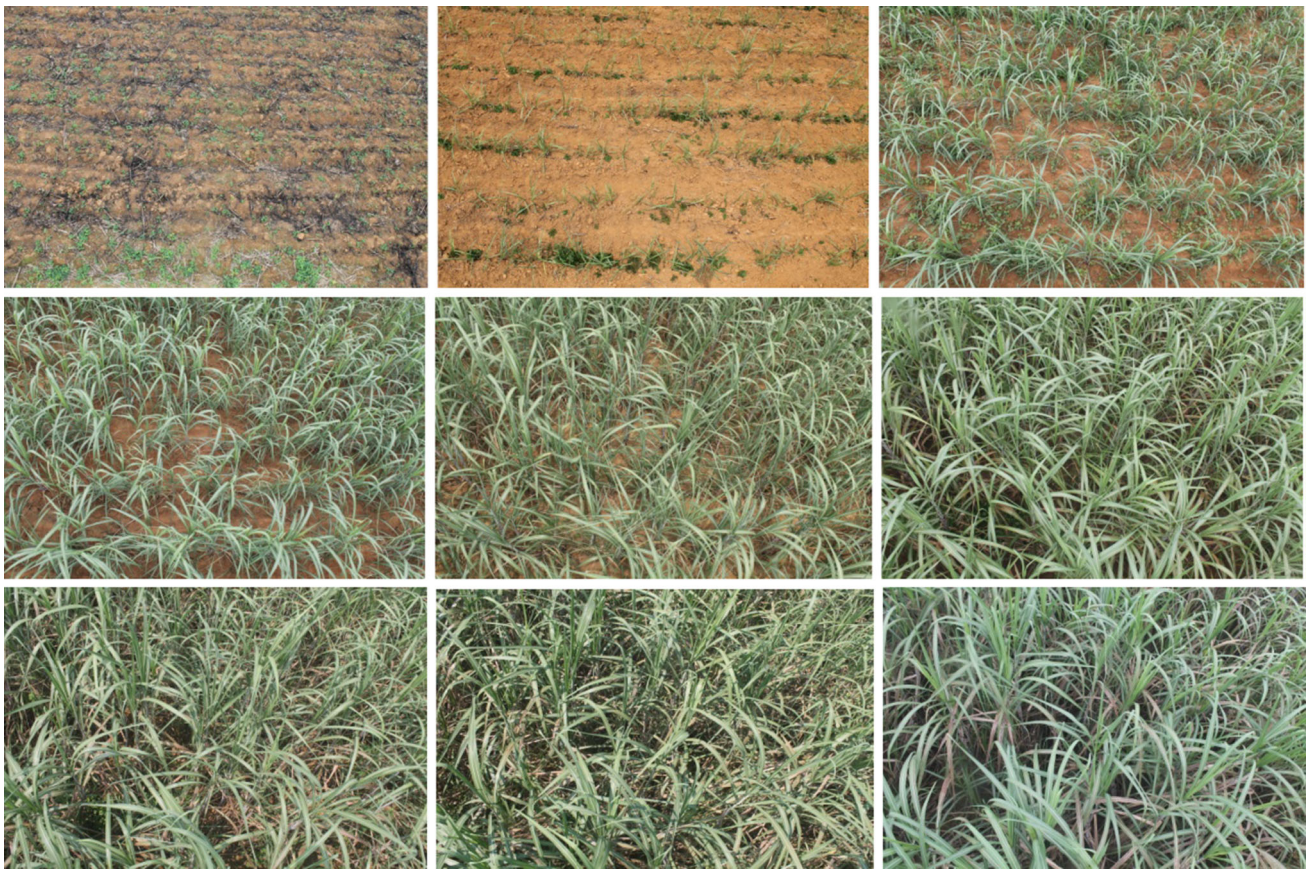

Fig. 7 Pictures of sugarcane canopy at different periods (top to bottom: row 1 from March to May, row 2 from June to August, row 3 from September to November)

113 d, 129 d, 145 d, 193 d and 209 d according to the threshold of NDVI change rate made for sample automatic training. The identification accuracy was evaluated through the calculation of the confusion matrix using sugarcane sampling points and non-sugarcane sampling points selected from field investigation and visual interpretation. The overall identification accuracies of sugarcane of 97 d remote sensing image to 113 d, 129 d, 145 d, 193 d and 209 d were 92.17%, 92.58%, 91.78%, 90.52% and 91.17%, respectively, and the identification results were ideal (Table 6 and Fig. 9).

The sugarcane sampling points for accuracy verification were classified by combining with DEM to clarify the sugarcane identification accuracies in plains, hills and mountains. The average identification accuracies of the 5 time phases in plains, hills and mountains were 95.61%, 91.84% and 83.80%, respectively, in which the identification accuracy of sugarcane in plains was the highest (Table 6).

In order to understand the applicability of the analysis and obtained result in 2011, the sugar cane identification model and indicators established in this paper were used to identify sugarcane of test area during spring and summer season in 2017 (Fig. 10). In the spring (97–113 d and 97–145 d) of 2017, the overall recognition accuracy of sugarcane was 88.44% and 89.79%, respectively. Meanwhile, in the summer (97–193 d and 97–209 d), the overall recognition accuracy of sugarcane was 87.79% and 88.34%, respectively (Table 7).

It can be seen that the sugarcane identification model and indicators established in this study have also achieved good results in other years, but the overall recognition accuracy is declining. If the accuracy is to be improved, the sugarcane samples must be reanalyzed and the index threshold adjusted. This is because the growth of sugarcane in 2011 may be different from that of other years, and some areas are no longer sugarcane areas due to the change of planting structure.

Conclusions

In this study, we found that ESTRAFM can generate high-quality and high-resolution data. The ESTRAFM model is used to carry out the fusion of MODIS and HJ-1 CCD data, producing the 30 m resolution NDVI series images of the

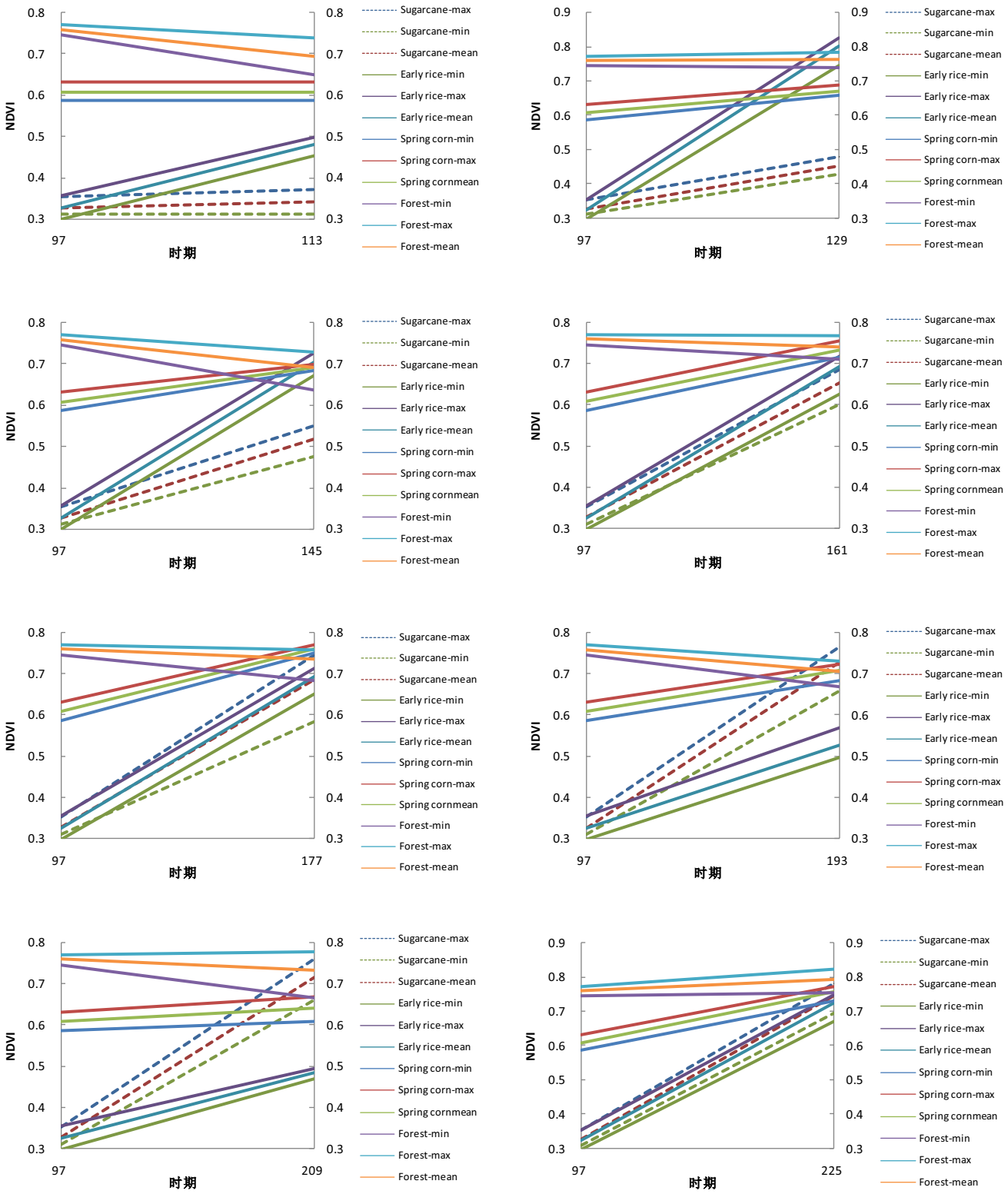

Fig. 8 Changes in NDVI of different vegetations in different periods in the test area

whole growth period of sugarcane, which provides reliable data for the timely and refined identification of sugarcane planting information in spring and summer. The fused images show high similarity to the observed images, indication good fusion quality. The correlation coefficient in the sugarcane planting area is 0.953, and AD, AAD and

Table 5 Threshold value of NDVI change rate for sugarcane identification in the test area

Period	*V*	$NDVI_t$
97–113 d	− 0.0005 to 0.0015	< 0.4
97–129 d	0.003–0.004	–
97–145 d	0.003–0.0045	–
97–193 d	0.003–0.0045	–
97–209 d	0.003–0.004	–

SD are 0.033, 0.019 and 0.007, respectively. According to the NDVI characteristics and change rules of sugarcane, the identification model for sugarcane in spring and summer is constructed by using the NDVI change rates of sugarcane from the emergence to the stem elongation stages, and the threshold of automatic training model is collected in the field. The model is used to identify the sugarcane planting information in different time phases of 113 d, 129 d, 145 d, 193 d and 209 d in spring and summer, and the overall accuracies are 92.17%, 92.58%, 91.78%, 90.52% and 91.17%, respectively. The established model also achieved good results in 2017 with the overall accuracies are 88.44%, 87.79%, 89.79%, 88.34% for 113 d, 145 d, 193 d and 209 d. Therefore, we concluded that the established sugarcane recognition model are ideal, which can provide a new way to achieve the timely and

Table 6 Accuracy evaluation of classification results in 2011

Data time phase	Total accuracy (%)	Kappa coefficient	Plain	Hill	Mountain
97–113 d	92.17	0.8756	96.17	92.73	84.07
97–129 d	92.58	0.8824	96.38	92.2	85.08
97–145 d	91.78	0.8645	95.73	92.25	84.38
97–193 d	90.52	0.8578	94.82	91.18	82.32
97–209 d	91.17	0.8632	94.97	90.86	83.17
Average	91.64	0.8687	95.61	91.84	83.80

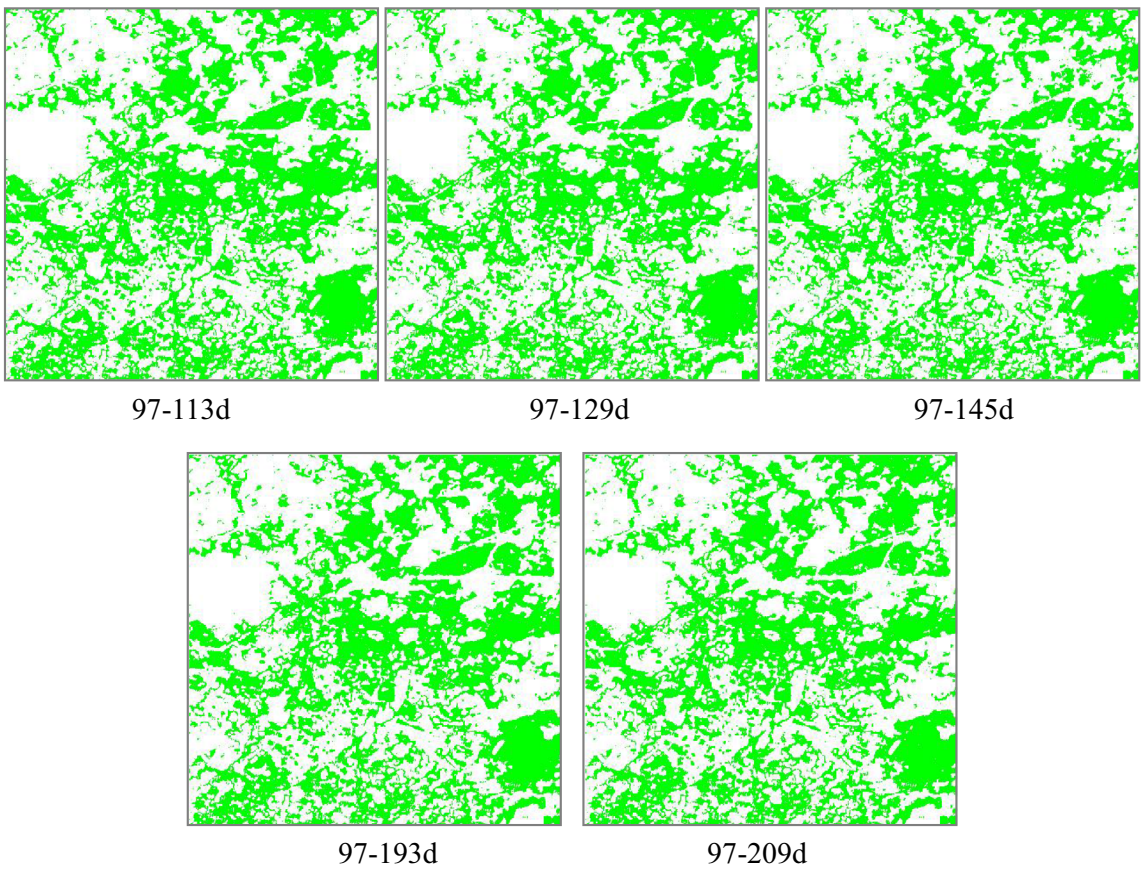

Fig. 9 Sugarcane identification result of test area province in 2011

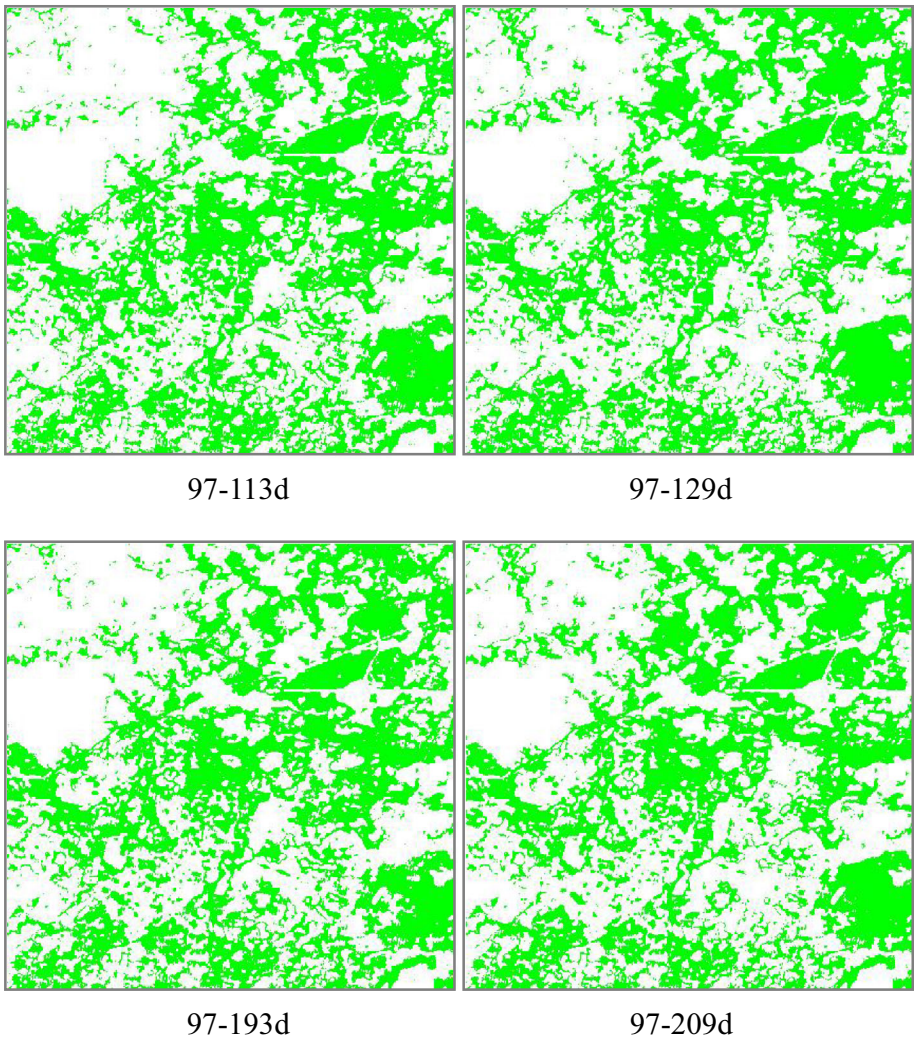

Fig. 10 Sugarcane identification result of test area province in 2017

Table 7 Accuracy evaluation of classification results in 2017

Data time phase	Total accuracy (%)	Kappa coefficient	Plain	Hill	Mountain
97–113 d	88.44	0.8466	92.55	87.60	82.31
97–145 d	87.79	0.8451	91.86	87.10	81.85
97–193 d	89.79	0.8539	92.78	88.24	83.20
97–209 d	88.34	0.8478	92.43	86.92	82.19
Average	88.59	0.84835	92.41	87.47	82.39

refined monitoring of sugarcane using optical remote sensing data in spring and summer.

Discussion

The reflectance of the central pixel of high-resolution image fused from ESTRAFM model is determined by the similar pixel in the low-resolution image. Thus, the accuracy of the similar pixel selection determines the accuracy of the fused image. However, due to the coarse scale of low-resolution images and the scattered planting of sugarcane in some regions, it is easy to have "the same spectrum with different objects" at the junctions of different vegetation types caused by adjacent terrains. Therefore, it is necessary to introduce other auxiliary information to improve the fusion effect of the fused image on the sugarcane area in further research.

For the identification model for spring and summer sugarcane planting information constructed from NDVI change rates and sample automatic training threshold, the setting of the change rate threshold is the key to the identification accuracy. The analysis on the identification accuracy of sugarcane at different landforms of plains, hills and mountain shows that the selection and distribution of samples have an important effect on the identification accuracy. However, the limited samples selected in this study have limitations. Therefore, it is necessary to conduct threshold training for more sugarcane samples with different growth vigor at different landforms in the test area for the sugarcane identification in much wider ranges. Moreover, due to the effects of revisiting cycle and cloudy and rainy weather, the spring and summer HJ-1 CCD data in the test area is seriously deficient. For example, there are only clear-sky images for April 19 and May 28 in 2011 for the test area, making it hard to carry out the systematic analysis on the sugarcane identification accuracy of the images with corresponding time before and after fusion. In the further research, the difference between the fusion images and original images of sugarcane recognition accuracy can be further analyzed, which will lay a foundation for improving the fusion model and obtain the fusion image of sugarcane area with higher accuracy.

Acknowledgements The authors thank the China centre for resources satellite data and application for providing HJ-1 CCD remote sensing data and technical support.

Funding Part of this research was jointly supported by the Guangxi Natural Science Foundation (No. 2018GXNSFAA281338); Drought Meteorological Science Research Foundation (No. IAM201707); Guangxi Natural Science Foundation (No. 2017GXNSFBA198153); National Key Basic Research Development Plan (No. 2013CB430205).

References

Alexandre, C. X., Bernardo, F. T., Yosio, E. S., Luciana, M. S. B., & Mauricio, A. M. (2006). Multi-temporal analysis of MODIS data to classify sugarcane crop. *International Journal of Remote Sensing, 27*(4), 755–768.

Cai, D. W., Niu, Z., Wang, L., & Li, Wang. (2012). Adaptability research of spatial and temporal remote sensing data fusion technology in crop monitoring. *Remote Sensing Technology and Application, 27*(06), 927–993.

Chen, L. F., Lin, K. P., Hu, B. Q., Li, J. J., & Ning, W. Y. (2015). Monitoring of sugarcane planting area based on landsat8_OLI data. *Journal of Southern Agriculture, 46*(11), 2068–2072.

Ding, M. H., Tan, Z. K., Li, H., Yang, Y. H., Zhang, H. Q., Mo, J. F., et al. (2012). Survey methods of sugarcane plant area based on HJ-1 CCD data. *Chinese Journal of Agrometeorology, 33*(2), 265–270.

Fortes, C., & Demattê, A. M. (2006). Discrimination of sugarcane varieties using Landsat 7 ETM+ spectral data. *International Journal of Remote Sensing, 27*(7), 1395–1412.

Gao, F., Masek, J., Schwaller, M., & Hall, F. (2006). On the blending of the Landsat and MODIS surface reflectance: Predicting daily Landsat surface reflectance. *IEEE Transactions on Geoscience and Remote Sensing, 44*(8), 2207–2218.

Jakubauskas, M. E., Legates, D. R., & Kastens, J. H. (2002). Crop identification using harmonic analysis of time-series AVHRR NDVI data. *Computers & Electronics in Agriculture*, *37*(1–3), 127–139.

Li, X. C., Xu, X. G., Wang, J. H., Jin, L. X., Li, C. J., & Bao, Y. S. (2013). Crop classification recognition based on time-series images from HJ satellite. *Transactions of the Chinese Society of Agricultural Engineering, 29*(2), 169–176.

Lin, H., Chen, J. S., Pei, Z. Y., Zhang, S. L., & Hu, X. Z. (2009). Monitoring sugarcane growth using ENVISAT ASAR data. *IEEE Transactions on Geoscience and Remote Sensing, 47*(8), 2572–2580.

Liu, J. K., Zhong, S. Q., Xu, Y., & Chen, Y. L. (2014). Sugarcane extraction in the southern hills using multi-temporal GF-1 WFV data. *Guangdong Agricultural Sciences, 41*(18), 149–154.

Ma, S. J., Pei, Z. Y., Wang, Q. F., Guo, L., Liang, Z. L., & Teng, D. J. (2011). Research of sugarcane harvest process monitoring with multi-temporal HJ—a satellite data. *Transactions of the Chinese Society of Agricultural Engineering, 27*(3), 215–219.

Miao, C. C., Jiang, N., Peng, S. K., Lv, H., Li, Y., Zhang, Y., et al. (2011). Extraction of paddy land area based on NDVI time-series data: Taking Jiangsu Province as an example. *Journal of Geo-Infomation Science, 13*(2), 273–280.

Sun, R., Rong, Y., Su, H. B., & Chen, S. H. (2016). NDVI time-series reconstruction based on MODIS and HJ-1 CCD data spatial–temporal fusion. *Journal of Remote Sensing, 20*(3), 361–373.

Tan, Z. K., Wu, L. L., Ding, M. H., Yang, X., Ou, Z. R., He, Y., et al. (2007). Study on the extraction of sugarcane planting area from EOS/MODIS data. *Meteorological Monthly, 33*(11), 76–81.

Vieira, M. A., Formaggio, A. R., Rennó, C. D., Atzberger, C., Aguiar, D. A., & Mello, M. P. (2012). Object based image analysis and data mining applied to a remotely sensed landsat time-series to map sugarcane over large areas. *Remote Sensing of Environment*, *123*, 553–562.

Wang, J. L., Huang, J. L., Wang, L. H., Hu, Y. X., Han, P. P., & Huang, W. (2014). Identification of sugarcane based on object-oriented analysis using time-series HJ CCD data. *Transactions of the Chinese Society of Agricultural Engineering, 30*(11), 145–151.

Wu, M. Q., Niu, Z., & Wang, C. Y. (2010). Mapping paddy fields by using spatial and temporal remote sensing data fusion technology. *Transactions of the Chinese Society of Agricultural Engineering, 26*(7), 240–244.

Yang, Y. J., Zhan, Y. L., Tian, Q. J., Gu, X. F., Yu, T., & Wang, L. (2015). Crop classification based on GF-1/WFV NDVI time series. *Transactions of the Chinese Society of Agricultural Engineering, 31*(24), 155–161.

Zhang, M., & Zeng, Y. N. (2015). Mapping paddy fields of Dongting Lake area by fusing Landsat and MODIS data. *Transactions of the Chinese Society of Agricultural Engineering, 31*(13), 178–185.

Zhang, X., Sun, R., Zhang, B., & Tong, Q. X. (2008). Land cover classification of the north China plain using MODIS_EVI time series. *ISPRS Journal of Photogrammetry & Remote Sensing, 63*(4), 476–484.

Zhou, Z., Huang, J. F., Wang, J., Zhang, K. Y., Kuang, Z. M., Zhong, S. Q., et al. (2016). Object-Orented classification of sugarcane using time-series middle-resolution remote sensing data based on adaboost. *PLoS ONE, 10*(11), e0142069. https://doi.org/10.1371/journal.pine.0142069.

Zhu, X. L., Chen, J., Gao, F., Chen, X. H., & Masek, J. G. (2010). An enhanced spatial and temporal adaptive reflectance fusion model for complex heterogeneous regions. *Remote Sensing of Environment, 114*(11), 2610–2623.